

# Crystal Structure of the Ribosome at 5.5 Å Resolution

Marat M. Yusupov,<sup>1\*</sup> Gulnara Zh. Yusupova,<sup>1\*</sup> Albion Baucom,<sup>1</sup>  
Kate Lieberman,<sup>1</sup> Thomas N. Earnest,<sup>2</sup> J. H. D. Cate,<sup>3†</sup>  
Harry F. Noller<sup>1†</sup>

We describe the crystal structure of the complete *Thermus thermophilus* 70S ribosome containing bound messenger RNA and transfer RNAs (tRNAs) at 5.5 angstrom resolution. All of the 16S, 23S, and 5S ribosomal RNA (rRNA) chains, the A-, P-, and E-site tRNAs, and most of the ribosomal proteins can be fitted to the electron density map. The core of the interface between the 30S small subunit and the 50S large subunit, where the tRNA substrates are bound, is dominated by RNA, with proteins located mainly at the periphery, consistent with ribosomal function being based on rRNA. In each of the three tRNA binding sites, the ribosome contacts all of the major elements of tRNA, providing an explanation for the conservation of tRNA structure. The tRNAs are closely juxtaposed with the intersubunit bridges, in a way that suggests coupling of the 20 to 50 angstrom movements associated with tRNA translocation with intersubunit movement.

Ribosomes are large ribonucleoprotein complexes that are responsible for protein synthesis in all cells. Unlike other cellular polymerases, their mechanism of action appears to be based fundamentally on RNA; i.e., they are ribozymes (1–3). Understanding the structural basis for the functional capabilities of rRNA is essential to explain why these ancient organelles use RNA, instead of protein, for the complex and biologically crucial task of translation. Bacterial ribosomes, which have been the most extensively investigated, are composed of small (30S) subunits, containing 16S rRNA and about 20 proteins, and large (50S) subunits, which contain 23S rRNA, 5S rRNA, and over 30 proteins (4). The complete 70S ribosome is formed by association of the 30S and 50S subunits through a network of intermolecular bridges (5). Its intersubunit space is occupied by the transfer RNAs (tRNAs), whose anticodons base pair with messenger RNA (mRNA) codons in the 30S subunit, whereas their 3'-CCA ends, which carry the growing polypeptide chain and the incoming amino acid, reach into the 50S subunit, the location of the peptidyl transferase center, where peptide bond formation is catalyzed.

The structure of the ribosome began to

emerge from the efforts of electron microscopists, using methods such as immunoelectron microscopy (IEM) to identify the locations of the different macromolecular components at low resolution [reviewed in (6)]. Classical electron microscopy (EM) has given way to cryo-EM reconstruction methods, which have provided increasingly higher resolution views of the ribosome and its subunits and functional complexes (5, 7, 8). More recently, the possibility of obtaining atomic-resolution structures of the ribosome by x-ray crystallography has come from the ability to prepare well-diffracting crystals of ribosomes and subunits (9) and to overcome the daunting phase problem (10–12). During the past year, this has led to high-resolution structures of *Haloarcula marismortui* 50S subunits (13) and of *Thermus thermophilus* 30S subunits (14, 15), providing detailed views of these vast and intricate ribonucleoprotein complexes. In addition, the structures of peptidyl transferase substrate analogs bound to the 50S subunit (3) and of a rRNA stem loop bound to the P site of the 30S subunit (16) begin to suggest how the ribosome interacts with tRNA at atomic resolution.

Previously, we described the cocrystallization of complete *T. thermophilus* 70S ribosomes in functional complexes with mRNA and A-, P-, and E-site tRNAs and the solution of their crystal structures at resolutions of up to 7.8 Å (11). Here, we describe the three-dimensional structure of the 70S ribosome containing mRNA and tRNAs bound to the P and E sites at 5.5 Å resolution and to the A site at 7 Å resolution. Features of the 50S subunit that were disordered in the high-resolution *Haloarcula* structure are found to be ordered in the 70S *Thermus* structure, providing a nearly complete view of the 50S

subunit. The three tRNAs are closely juxtaposed with certain intersubunit bridges, as suggested by chemical probing and cross-linking studies (17–20) and in previous cryo-EM and x-ray structures (11, 21). Several lines of evidence indicate that these bridges are mobile, suggesting that tRNA translocation is in some way coupled with intersubunit movement.

**Overall structure of the 70S ribosome.** *T. thermophilus* 70S ribosomes containing a synthetic mRNA analog and tRNAs bound to the P and E sites were crystallized as described earlier, and their diffraction was improved to 5 Å resolution (Table 1). Experimental phases to 7.5 Å were obtained from MAD experiments (11) and extended to an effective resolution of 5.5 Å by use of density modification algorithms involving solvent flipping (22) (Table 1). The quality of the phases was confirmed by the electron density of the bound tRNAs, which provided internal standards of known structure (Fig. 1). At 5.5 Å, the RNA backbones can be traced with high confidence, and proteins of known structure can be fitted readily to the electron density (23). Using 70S complexes crystallized with and without tRNA bound to the A site, we obtained a 7 Å Fourier difference map that provided the position of the A-site tRNA.

Figure 2A shows the structure of the 70S ribosome in the “standard view” from the solvent face of the 30S subunit, showing its head (H), body (B), platform (P), and neck (N) features and their corresponding 16S rRNA (cyan) and protein (blue) components. Jutting out at the lower right is the “spur” of the 30S subunit, formed by helix 6 of 16S rRNA, which makes a crystal contact with the P site of another subunit in the recently reported 30S subunit structure (16). In this view, the positions of proteins S2, S3, S9, S10, and S14 in the head; S6, S11, and S18 in the platform; and S4, S5, S8, and S16 in the body can be seen. In the background, parts of the 50S subunit are visible in the “crown” view, with its 23S rRNA (gray), 5S rRNA (top; blue), and 50S subunit proteins (magenta). Protein L9 can be seen at the left, extending more than 50 Å beyond the surface of the 50S subunit proper. On the upper left, L1 and its 23S rRNA binding site protrude outside the profile of the 30S subunit, and protein L11 and its RNA and one of the L7 dimers make up the stalk at the upper right.

From the right-hand side (Fig. 2B), the anticodon end of the A-site tRNA (gold) is visible in the near end of the subunit interface cavity, viewed through the large funnel-shaped opening where elongation factors EF-Tu and EF-G interact with the ribosome. One of the ribosomal structures that interacts with the G domains of the elongation factors is the sarcin-ricin loop (SRL) of 23S rRNA, which

<sup>1</sup>Center for Molecular Biology of RNA, Sinsheimer Laboratories, University of California at Santa Cruz, Santa Cruz, CA 95064, USA. <sup>2</sup>Berkeley Center for Structural Biology, Physical Biosciences Division, Lawrence Berkeley National Laboratory, Berkeley, CA 94720, USA. <sup>3</sup>Whitehead Institute, Cambridge, MA 02142, USA.

\*Present address: UPR 9004 de Biologie et de Genomiques Structurales du CNRS, IGBMC B.P. 163, 1 rue L. Fries, 67404 Illkirch Cedex—CU de Strasbourg, France.

†To whom correspondence should be addressed.

is visible between the A-tRNA and protein L14. Also evident in the right-hand view are proteins S9, S12, S13, S19, S20, L3, L5, L6, L7, L11, L13, L14, L19, L22, L25, and L30, as well as the positions of proteins L21 and L32 (whose structures are not known), and the positions of electron density labeled LU, LV, and LX that we ascribe to as yet unidentified large subunit ribosomal proteins (which may include the three unassigned known proteins L31, L35, and L36). 5S rRNA (5S) is visible at the top of the 50S subunit, along with two of its binding proteins, L5 and L25.

The view from the back of the 50S subunit (Fig. 2C) reveals the locations of additional 50S subunit proteins L4, L15, L16, L21, L24, L27, L28, L29, L32, L33, and L34, the third 5S rRNA-binding protein L18, and unidentified proteins LW and LY. The opening of the polypeptide exit channel (EC) is at the bottom of the back side of the 50S subunit, surrounded by proteins L22, L24, and L29 in addition to elements of domains I and III of 23S rRNA.

In the left-hand view (Fig. 2D), the close approach of the two subunits at the interface is much more evident. The platform of the 30S subunit, around proteins S11, S6, and S15, contacts the 50S subunit near protein L2, mainly through RNA-RNA interactions and RNA-protein interactions involving proteins S15 and L2. The E-site tRNA (red) can be seen at the near side of the interface cavity, partly shielded from view by L1 and its RNA binding site, which appear to block the path for its exit from the ribosome. In the top view (Fig. 2E), the orientations of all three tRNAs (A, gold; P, orange; and E, red) in the interface cavity can be seen more clearly. In this view, protein S13 in the head of the 30S subunit can be seen to contact helix 38 of 23S rRNA (the A-site finger; ASF) to form bridge B1a. Also evident is the close approach between proteins L5 and S13, whose electron densities merge to form the single protein-

protein intersubunit contact (bridge B1b), which lies directly above and parallel to the anticodon arm of the P-site tRNA (see below).

Viewed from the interface (Fig. 2, F and G), fewer proteins are visible on the 30S and 50S subunits, and they are located mainly around the periphery, leaving large exposed surfaces of ribosomal RNA. The three tRNAs are aligned on the 30S subunit with their anticodon ends bound in the RNA-rich groove between the head, body, and platform (Fig. 2F). The rest of all three tRNAs, including their D stems, elbows, and acceptor arms, interact with the 50S subunit. The acceptor arms of the A and P tRNAs point downward into the peptidyl transferase cavity, where their acceptor ends come within 5 Å of each other, whereas the E-tRNA acceptor arm is directed into a separate cleft next to the L1 ridge, placing its acceptor end nearly 50 Å from that of the P-tRNA. The tRNA binding site neighborhoods are dominated by rRNA, as are the interface contact surfaces.

The secondary structure of 16S rRNA (Fig. 3A) (24, 25) falls into four recognizable domains, called the 5', central, 3'-major and 3'-minor domains. As observed in the structures of the isolated ribosomal subunits (14, 15), the secondary structure domains of 16S rRNA (Fig. 3A) do indeed correspond to three-dimensional domains that are nearly structurally autonomous (Fig. 3C). This organization immediately suggests that the domains are designed to move relative to one

another during protein synthesis. In particular, the very minimal interaction between the head and the rest of the subunit is consistent with movement of the head during translocation (26-28). The four domains converge near the geometric center of the subunit, next to the sites of its functional interactions with mRNA and tRNA, further suggesting coupling of interdomain movement with biological function.

The more than 130 individual helices predicted from comparative sequence analysis of 23S rRNA (29) are found in its x-ray crystal structure, except for a predicted *Thermus*-specific helix inserted around position 650 of 23S rRNA, relative to the *Escherichia coli* secondary structure for which no electron density is found (25). The 23S rRNA and 5S rRNA together form seven secondary structural domains (Fig. 3B). In contrast to the design of the 30S subunit, the domains of 23S rRNA are extensively intertwined with each other, as first noted for the *H. marismortui* 50S subunit (13), creating the single large, hemispherical domain that forms the body of the 50S subunit (Fig. 3D). From the body project a number of molecular stalks, made up of RNA elements from domains II, IV, V, and VI, some of which are extended coaxial helical arms and others of which are mushroomlike globular RNA domains tethered to the body of the subunit by helical stems. Some of the stalks form bridges with the 30S subunit, whereas others interact with the tRNAs and elongation factors; the stalks are

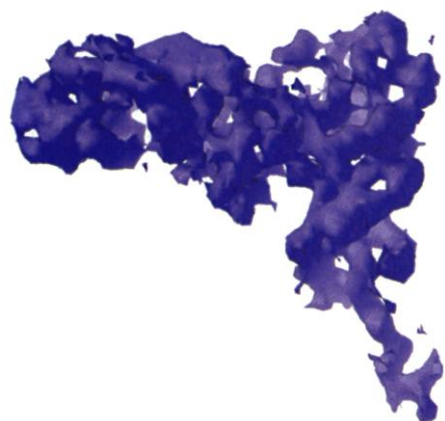


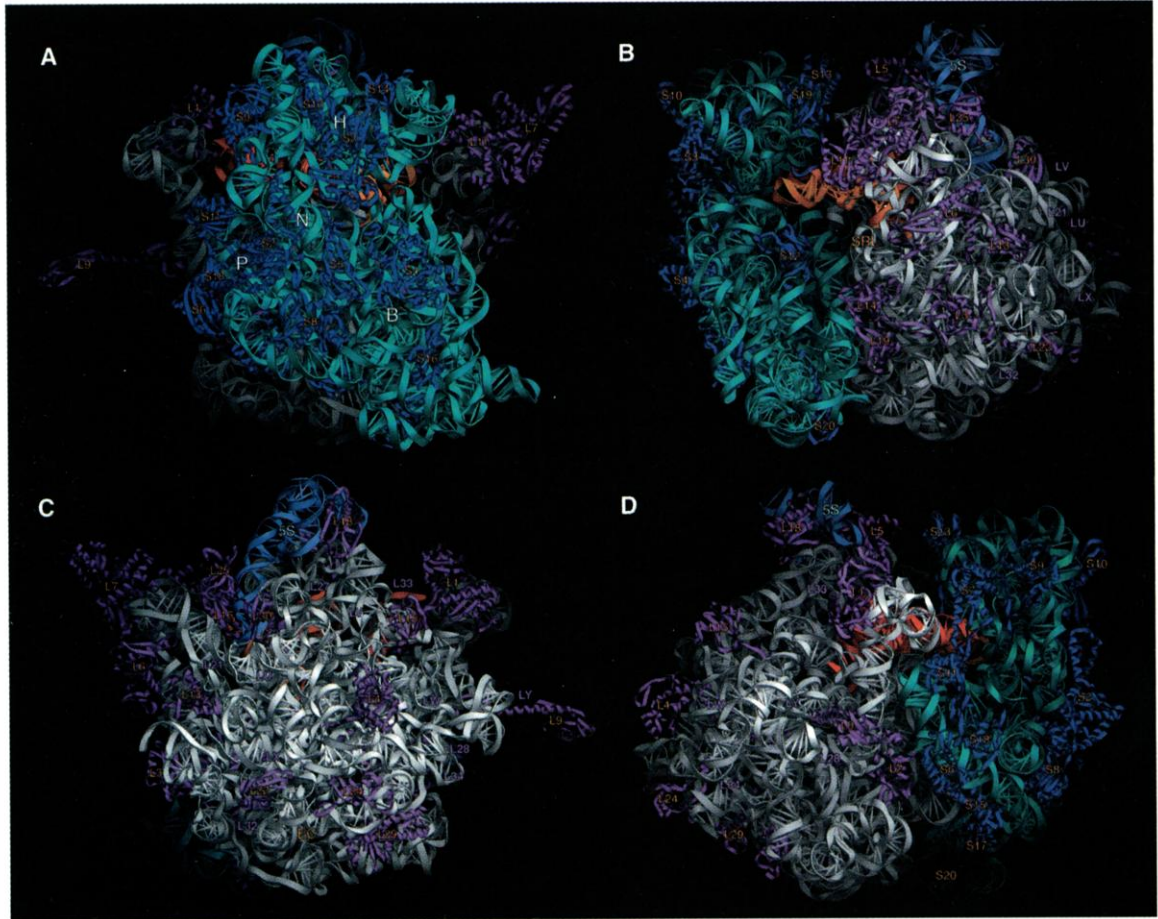
Fig. 1. Electron density of tRNA<sup>Met</sup> bound to the P site of the 70S ribosome, at 5.5 Å resolution.

**Table 1.** Crystallographic statistics and scaling. Crystals of *Thermus thermophilus* 70S ribosome functional complexes were grown as described (17). All complexes contained 70S ribosomes, a 36-mer mRNA fragment derived from phage T4 gene 32 mRNA, and a tRNA of unknown identity bound to the E site. The other ligands were as follows: (ASL), a synthetic 19-nucleotide analog of the tRNA<sup>Phe</sup> anticodon stem-loop bound to the 30S subunit P site; (P site), tRNA<sup>Met</sup> bound to the P site; (No mRNA), as for P site, except lacking the mRNA fragment; and (A site), as for P site, but also including tRNA<sup>Phe</sup> bound to the A site. Crystals grew in space group I422 with cell dimensions of  $a = b = 507.2$  Å and  $c = 803.7$  Å. Structure factor amplitudes were measured at the Advanced Light Source (ALS), essentially as described (17). Structure factor phases determined experimentally from a crystal containing an anticodon stem loop tRNA analog in the P site ("ASL") (17) were used as a starting point for structure factor phasing of diffraction data measured from crystals containing tRNA<sup>Met</sup> in the P site ("P site"). Phase extension to 5.0 Å was carried out by density modification and solvent flipping in CNS (22). The quality of the phases was assessed by monitoring the appearance of intact tRNA in the P site (Fig. 1).

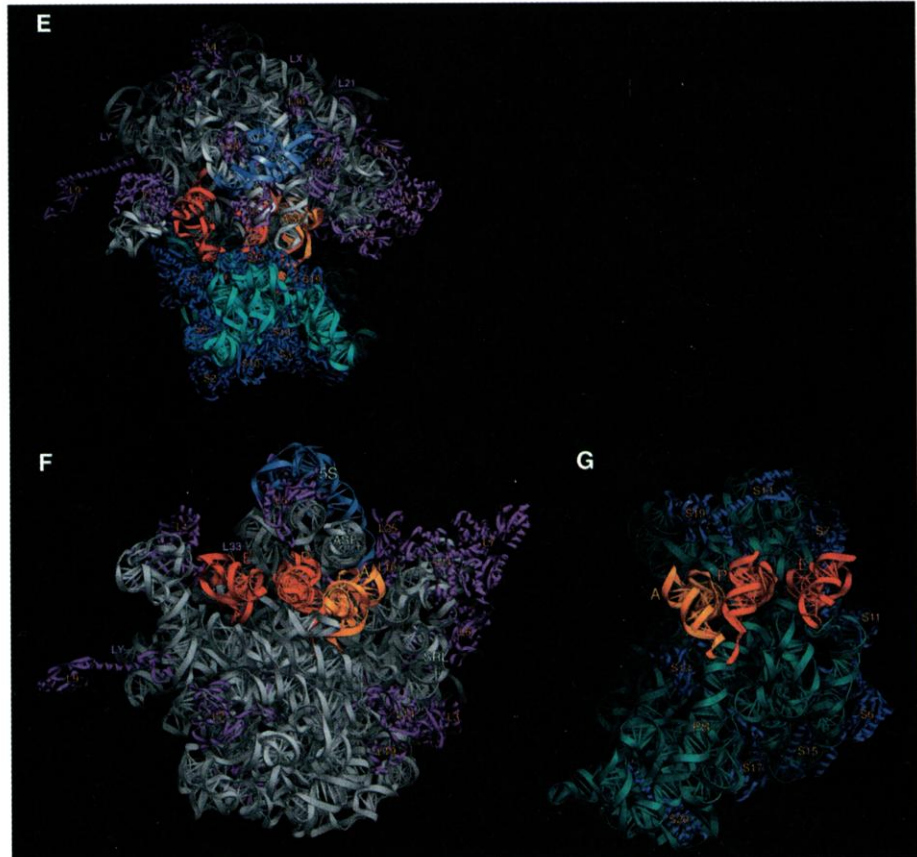
Crystal	ASL	P site	No mRNA	A site
High-resolution limit (Å)	7.5	5	6.5	6.5
$R_{\text{sym}}^*$	8.9	9.4	8.9	7.2
Mean $I/\sigma(I)$	3.1 (at 7.8 Å)	3.3 (at 5.5 Å)	4.4 (at 7.0 Å)	3 (at 7.0 Å)
Number of reflections				
Unique	124,437#	209,044	95,127	95,671
Observational redundancy	4.4	2.8	3.6	2.3
Completeness (%)	97.7	95.3	96.6	93.9
$R_{\text{iso}}^\dagger$ (%)		23.6		
$\chi^2$ , cross-crystal‡		36.9		
Mean figure of merit for starting phase set (at 7.5 Å)§		0.505		

\* $R_{\text{sym}} = \sum |I - \langle I \rangle| / \sum I$ . † $R_{\text{iso}} = \sum |F_{\text{PH}} - \langle F_{\text{P}} \rangle| / \sum F_{\text{PH}}$ , where  $F_{\text{PH}}$  and  $F_{\text{P}}$  are the structure factor amplitudes from the ASL-containing ribosome crystal and the P-site tRNA-containing ribosome crystal, respectively. ‡ $\chi^2$  analysis, from 20 to 7.5 Å, was taken from Scalepack (70). §The mean figure of merit, or mean cosine of the phase error, was calculated from experimental phases measured from the ASL-containing crystal (17). #Data set taken from the previously reported MAD phasing experiment (17).

**Fig. 2.** Views of the structure of the *T. thermophilus* 70S ribosome. (A) to (D) are successive 90° rotations about the vertical axis; (E) is a 90° rotation around the horizontal axis of the view shown in (A). (A) View from the back of the 30S subunit. H, head; P, platform; N, neck; B, body. (B) View from the right-hand side, showing the subunit interface cavity, with the 30S subunit on the left and the 50S on the right. The anticodon arm of the A-tRNA (gold) is visible in the interface cavity. (C) View from the back of the 50S subunit. EC, the end of the polypeptide exit channel. (D) View from the left-hand side, with the 50S subunit on the left and the 30S on the right. The anticodon arm of the E-tRNA (red) is partly visible. (E) View from the top, with the 50S subunit above and the 30S below. The E-, P-, and A-tRNAs are visible in the interface cavity with their anticodon arms pointed downward into the 30S subunit.



(G) Interface view of the 30S subunit [rotated 180° from (A)], showing the positions of the three tRNAs. (F) Interface view of the 50S subunit. ASF, A-site finger; SRL, sarcin-ricin loop. The different molecular components are colored for identification: cyan, 16S rRNA; gray, 23S rRNA; light blue, 5S rRNA (5S); dark blue, 30S proteins; magenta, 50S proteins. Proteins fitted to the electron density are numbered in orange; 50S proteins whose electron density has been identified but not fitted are numbered in magenta. A, P, and E are the A-, P-, and E-site tRNAs (gold, orange, and red, respectively).



likely to be dynamic elements of the 50S subunit, undergoing movement in connection with their various functional interactions, as discussed below.

**Differences between the conformations of 70S ribosomes and isolated subunits.** Comparison of the conformation of 16S rRNA in 70S ribosomes with that of the 30S subunit structure reported by Wimberly *et al.* (14) shows a nonuniform distribution of differences (Fig. 4A) (30). The highest values (>10 Å) are observed for the spur region (SP) in the lower left of the body; this difference can be explained by a crystal contact in which the spur helix binds to the P site of a symmetry-related subunit in the Wimberly *et al.* structure. The other major conformational differences (between 3.5 and 10 Å) are localized to a few regions, including the penultimate stem (PS), the top of the platform, and the head of the subunit. All of these features interact with the 50S subunit, as described below, suggesting that the observed differences may include conformational changes that occur upon subunit association. These same regions were found to differ in comparisons between cryo-EM maps and a 5 Å x-ray structure of the 30S subunit (8, 12).

Differences between the conformations of 23S rRNA in *T. thermophilus* 70S ribosomes and *H. marismortui* 50S subunits (13) are summarized in Fig. 4, B and C (30). Features of 23S rRNA that were disordered in the 50S structure (yellow) include several of the protruding stalk elements, including the L1 RNA and L11 RNAs, the A-site finger, and the 1915 stem loop. These elements are probably stabilized by interactions with the 30S subunit and with the tRNAs in the 70S ribosome complex. It is also possible that the inherent thermal stability of the *Thermus* ribosome contributes to the lower degree of disorder.

Many additional conformational differences with the *Haloarcula* 50S subunit are found (Fig. 4, B and C). Some differences are explained by expected phylogenetic structural variation between corresponding regions of the bacterial and archaeal RNAs. There are examples of RNA helices and other features that are specific to the bacterial structure (Fig. 4, B and C; cyan) and, conversely, ones that are specific to the archaeal structure (white). These phylogenetically variable features are located at the bottom and back surfaces of the subunit, remote from the subunit interface and functional sites.

#### Structures of the intersubunit bridges.

Intersubunit contacts were first visualized as discrete bridges in low-resolution cryo-EM studies and more recently at 11.5 Å resolution by Frank and co-workers (5, 8). In our previous 7.8 Å structure (11), at least 10 individual bridges could be resolved. At 5.5 Å, all of the molecular components involved in the intersubunit contacts can be identified,

including two additional protein-containing bridges. As inferred from earlier chemical probing (17, 18) and modification-interference (31) studies, most of the bridge contacts involve rRNA, as summarized in Fig. 5A. Figure 5C shows the 30S bridge contacts, viewed from the interface, with the anticodon stem loops of the A-, P-, and E-tRNAs in their respective 30S subunit binding sites. The distribution of RNA-RNA versus RNA-protein or protein-protein contacts is striking; the RNA-RNA contacts (magenta) are centrally located on the platform and penultimate stem, directly abutting the tRNA binding sites. In contrast, contacts involving proteins (yellow) are peripherally located, more distal from the functional sites. On the 50S subunit side (Fig. 5B), the RNA-RNA contacts are

again central, forming a triangular patch across the front surface of the interface wall that separates the peptidyl transferase and E sites from the interface cavity. The RNA-RNA interactions exclusively involve RNA elements from domain IV of 23S rRNA, except for a small RNA-RNA contact from helix 34 of domain II that makes up most of bridge B4 (32). The only other part of 23S rRNA involved in a bridge contact is the tip of helix 38 (the A-site finger), which forms the RNA-protein bridge B1a. The rest of the bridge interactions from the 50S subunit are made by proteins L2, L5, L14, and L19.

The molecular contacts forming the 12 intersubunit bridges (Fig. 5, B and C) are summarized in Table 2. Multiple contacts can be seen in the electron density map for many

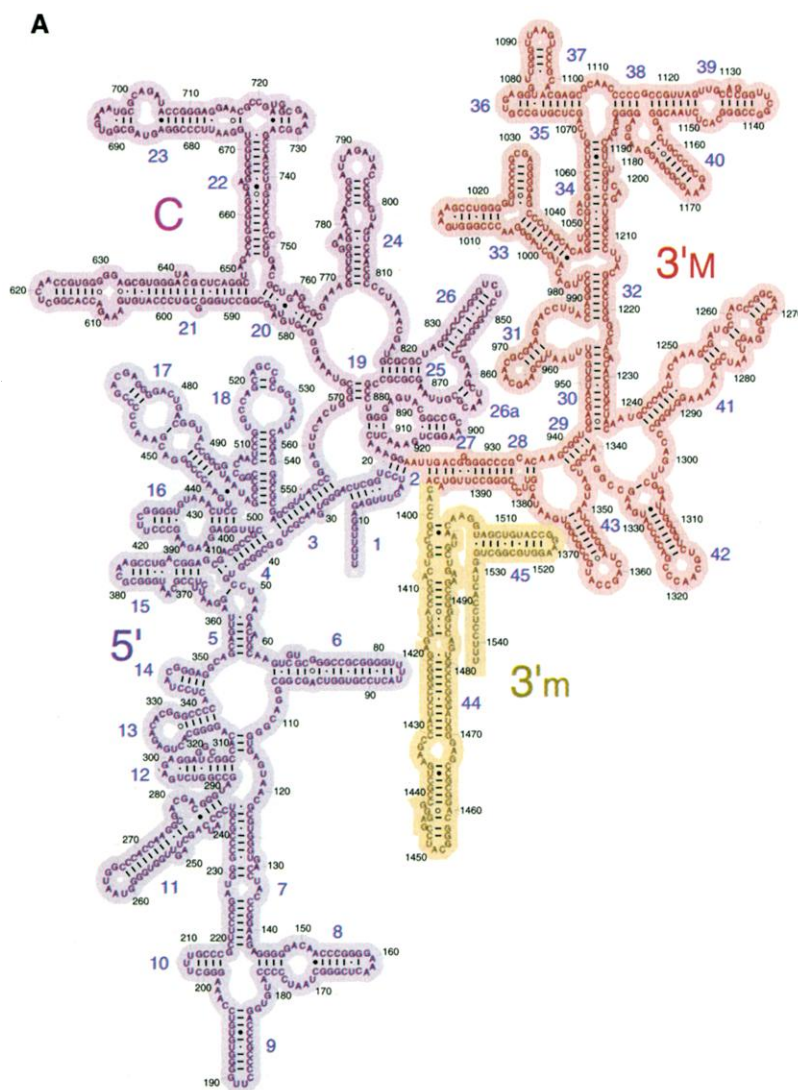


**Fig. 3.** Secondary and tertiary structures of 16S, 23S, and 5S rRNAs. (A) Secondary structure of *T. thermophilus* 16S rRNA, with its 5', central, 3'-major, and 3'-minor domains shaded in blue, magenta, red, and yellow, respectively. (B) Secondary structures of *T. thermophilus* 23S and 5S rRNAs, indicating domains I (blue), II (cyan), III (green), IV (yellow), V (red), and VI (magenta) of 23S rRNA. The rRNAs are numbered according to *E. coli* (69). (C) Three-dimensional fold of 16S rRNA in 70S ribosomes, with its domains colored as in (A). (D) Three-dimensional folds of 23S and 5S rRNAs, with their domains colored as in (B).

RESEARCH ARTICLES

of the bridges, giving a total of more than 30 individual interactions. RNA-RNA contacts are dominated by minor groove-minor groove interactions, although major groove, loop, and backbone contacts are also found.

The bridge proteins make use of virtually all types of RNA features for recognition, including major groove, minor groove, backbone, and loop elements.

Bridges B1a and B1b connect the head of

the 30S subunit to the top of 50S subunit, crossing the interface directly above and parallel to the A- and P-tRNAs (Fig. 2E). B1a, which has been called the "A-site finger" (5) is mostly disordered in the *Haloarcula* 50S

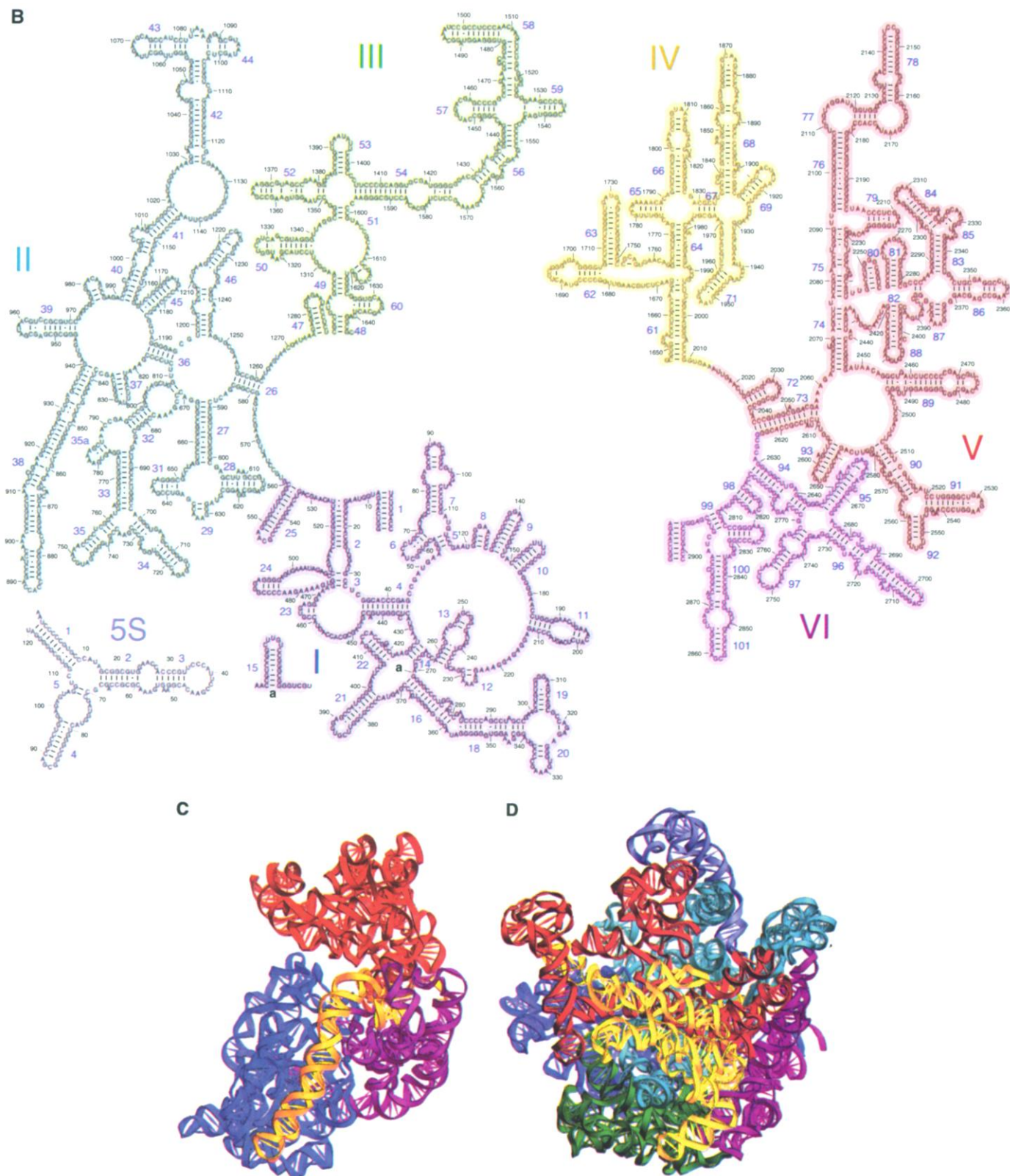


Fig. 3. (continued).

subunit structure (13). It consists of a long helical RNA arm (helix 38 of 23S rRNA) reaching from the right side of the central protuberance of the 50S subunit to the middle of the head of the 30S subunit, where its apical 890 loop contacts the conserved basic sequence around position 92 of protein S13. Bridge B1b is the sole protein-protein contact between the subunits. Helix 84 of 23S rRNA reaches partway toward the head of the 30S subunit above the P-tRNA; the remaining distance is bridged by protein L5, which contacts the NH<sub>2</sub>-terminal tail of S13 from a 20-amino acid loop formed by residues 134 to 153 of L5 (Hm positions 109 to 127), which are also disordered in the *H. marismortui* 50S structure.

Bridges B2a, B3, B5, and B6 (Fig. 5, B and C) all involve interactions between the 50S subunit and the penultimate stem (helix 44) of 16S rRNA, the dominant structural component of the 30S subunit interface. Figure 5D shows the arrangement of the RNA elements forming these four bridges. At the top, bridge B2a is made by the 1914 loop of helix 69 of 23S rRNA, another feature that is disordered in the *Haloarcula* 50S subunit structure. It contacts the decoding site of 16S rRNA around position 1408, as predicted from cross-linking experiments (19) in the first of a series of three consecutive minor groove-minor groove interactions. In the next one (B3), helix 71 of 23S rRNA contacts the penultimate stem at its two consecutive noncanonical A-G pairs around position 1418. Just below B3, a major groove contact (B5) is made by the minor groove of helix 64 of 23S rRNA, followed by the third minor-minor interaction (B6) formed by contact with helix 62. A further contact with the penultimate stem at bridge B6 is made by protein L19 (Fig. 5E). L14, which interacts with L19 by forming an intermolecular  $\beta$ -sheet, contacts the major groove side of the 345 loop of helix 14 of 16S rRNA to form bridge B8 (Fig. 5E).

Helices 68 and 71 of 23S rRNA form a long, largely noncanonical coaxial arm that lies horizontally along the top of the interface wall of the 50S subunit, containing the 50S components of bridges B2b and B7a, in addition to the aforementioned B3 (Fig. 5C). Figure 5F shows the complex set of interactions that form B2b and B7a, viewed from the top of the platform. The electron density for bridge B7a suggests that A702, which is strongly protected from diethyl pyrocarbonate modification in 70S ribosomes (18), makes an "A-minor" contact (32a) with the minor groove of helix 68 of 23S rRNA. The two remaining protein-RNA bridges are shown in Fig. 5G. Protein L2 makes two distinct contacts with 16S rRNA (B7b), at helices 23 and 24; L2 is also very close to protein S6 (not shown in figure) and may

make transient contacts with it during translation. The proposed role of L2 in peptidyl transferase activity (33) might be related to its participation in bridge B7b, which could serve as a relay between tRNA interactions in the small subunit and the catalytic center in the large subunit. Bridge B4 is primarily an interaction between protein S15 and the 715 loop of helix 34 of 23S rRNA, as shown previously (32); the 715 loop also makes a modest RNA-RNA contact with helix 20 of 16S rRNA (Fig. 5G).

**tRNA-ribosome interactions.** Most important for understanding the translational mechanism is how the ribosome interacts with its substrates, the tRNAs. In addition to their well-known interactions with mRNA, through base pairing between the codons and anticodons, tRNAs also interact with the ribosome itself. These interactions not only help to stabilize the binding of tRNA to the ribosome but are involved directly in functional processes such as discrimination mechanisms that increase the accuracy of aminoacyl-tRNA selection, maintaining the correct translational reading frame, translocational movement of tRNAs within the ribosome, and catalysis of peptide bond formation. Knowledge of the molecular contacts between tRNA and the ribosome thus provides

a structural framework for elucidation of mechanisms for these processes. As predicted by many earlier studies [reviewed in (2)], the tRNAs are mainly surrounded by elements of rRNA in the ribosome, most of which were identified in footprinting, cross-linking, and directed hydroxyl radical probing studies (20, 34, 35). Not surprisingly, we find that all three tRNA binding sites (A, P, and E) of the ribosome contact all three tRNAs at universally conserved parts of their structures; this allows the ribosome to bind different tRNA species in precisely the same way.

The A-tRNA density could be fitted to the structure of tRNA<sup>Phe</sup> (36) without modification, whereas the P-tRNA is kinked slightly around the junction of the D and anticodon stems, angling the anticodon loop toward the A site and narrowing the major groove of the anticodon stem. The E-tRNA is substantially distorted relative to known tRNA crystal structures. The angle of its elbow is more open, and the anticodon stem pivots near its junction with the D stem, pinching the major groove of the D stem. Its anticodon loop makes an unusually sharp U-turn.

Figure 6A shows the electron density of the A- and P-tRNAs bound to their respective codons, and Fig. 6B shows the overall relative geometry of the A-, P-, and E-tRNAs and

**Table 2.** Intersubunit bridges. Bridges are numbered B1a, B1b, etc., as shown in Fig. 5, B and C. rRNA contacts are to 16S rRNA for the 30S subunit and to 23S rRNA for the 50S subunit, listed by the number of the proximal helix (H44, etc.), numbered as shown in Fig. 3, A and B. rRNA nucleotide numbers are according to *E. coli* numbering. Molecular contacts are scored in parentheses as follows: M, major groove; m, minor groove; L, loop; B, backbone; Lm refers to the minor groove side of the loop, LB to the loop backbone, etc.

Bridge	Type	30S subunit		50S subunit	
		16S rRNA helix or S protein	RNA or protein positions	23S rRNA helix or L protein	RNA or protein positions
B1a	Prot-RNA	S13	92–94	H38(L)	886–888
B1b	Prot-Prot	S13	NH <sub>2</sub> -term	L5	134–153
B2a	RNA-RNA	H44(m)	1408–1410, 1494–1495	H69(Lm)	1913–1914, 1918
B2b	RNA-RNA	H24(m,Lm)	784–785,794	H67(m), H69(M)	1836–1837, 1922
	RNA-RNA	H45(LM,Lm)	1516–1519	H71(M), H69(B)	1919–1920, 1932
B2c	RNA-RNA	H24(Bm)	770–771	H67(B)	1832–1833
	RNA-RNA	H27(Bm)	900–1	H67(B)	1832–1833
B3	RNA-RNA	H44(m)	1484–1486	H71(m)	1947–1948, 1960–1961
B4	RNA-RNA	H20(m)	763–764	H34(Lm)	717–718
	Prot-RNA	S15	40–44, COOH-term	H34(LB,Lm)	713, 717
B5	RNA-RNA	H44(m)	1418–1419	H64(m)	1768–1769
	RNA-Prot	H44(B)	1420–1422	L14	44–49
	RNA-RNA	H44(B)	1474–1476	H62(Bm)	1689–1690
	RNA-RNA	H44(B)	1474–1476	H64(m)	1989
B6	RNA-RNA	H44(m)	1429–1430, 1474–1476	H62(m)	1689–1690, 1702–1705
	RNA-prot	H44(B)	1431	L19	(Hm24e;R44)
B7a	RNA-RNA	H23(L,m)	698,702	H68(m)	1848–1849, 1896
B7b	RNA-Prot	H23(M,m)	712–713	L2	162–164, 172–174, 177–178
	RNA-Prot	H24(M,m)	773–776	L2	177–178, 198–202
B8	RNA-Prot	H14(LM)	345–347	L14	116–119

the mRNA as they are positioned in the 70S ribosome crystals. Their specific contacts with the ribosome indicate that they are in their “classical” (A/A, P/P, and E/E), rather than hybrid binding states (37). All three tRNAs are shared between the two ribosomal subunits in a similar way; their anticodon stem loops are bound by the 30S subunit, and contacts with the rest of the tRNA—D stem, elbow, and acceptor arm—are made by the 50S subunit. The planes of the A- and P-tRNAs form an included angle of 26°, and the P- and E-tRNAs form an angle of 46°. The closest approach between the backbones of the anticodon stem loops of the A- and P-tRNAs is about 10 Å, a surprisingly large distance, in view of the fact that these two tRNAs read adjacent codons on the mRNA. The simultaneous reading of the two codons is accommodated by a kink in the mRNA backbone of about 45° between the A and P codons (Fig. 6B). The A- and P-tRNA backbones are closest at the acceptor stems, which approach within 5 Å of each other. At the elbow, the bases D16 of A-tRNA and U47 of P-tRNA are actually within H-bonding distance of each other, although we are not aware of prior evidence that such an interaction takes place. The CCA tails of the A- and P-tRNAs converge, as expected, at their 3' ends in the peptidyl transferase site of the 50S subunit. The closest approach of the anticodon stem backbones of the P- and E-tRNAs is about 6 Å, closer than found for the A- and P-tRNAs. However, the elbow and acceptor arm of the E-tRNA are rotated substantially away from the P-tRNA, so that their respective 3' ends are nearly 50 Å apart. The distances between corresponding positions of the three tRNAs are a measure of the magni-

tude of the movement of tRNA during translocation. Thus, the anticodon end of tRNA moves about 28 Å between the 30S A and P sites, and 20 Å between the P and E sites. Because of the rotation of the plane of the tRNA, the elbow moves through much larger distances of 40 and 55 Å, as it transits from A to P to E.

As observed previously, the anticodon stem loop (ASL) of P-tRNA and P codon is positioned by six sets of interactions (a to f) with the 30S subunit (11). The structural features involved in these interactions are shown in Fig. 6, C and D, and summarized in Table 3 (38). The mode of binding of the anticodon stem loop and its contacts are very similar to those previously observed for binding of helix 6 to the 30S P site (16). All six of the 30S P-site interactions involve direct contacts with 16S rRNA, two of which (a and d) are bolstered by interactions with the extended COOH-terminal tails of proteins S13 and S9, respectively. The phylogenetically somewhat variable lysine-rich tail of S13 interacts with phosphate 36 of the P-tRNA. In contrast, the tail of S9 is precisely conserved, and its COOH-terminal arginine, which appears to interact with phosphate 35 in the anticodon of P-tRNA, is universally conserved. These same phosphates were identified in phosphorothioate-interference experiments to be important for binding to the 30S P site (39). One of the earliest experiments implicating rRNA in ribosome function was the demonstration that kethoxal modification of a limited number of guanines in 16S rRNA caused loss of P-tRNA binding to the 30S subunit (40). Of the five 16S rRNA bases that interact with the P-site mRNA-tRNA complex, G926, 2mG966, G1338, A1339, and C1400, three

are guanines, explaining the early findings. Moreover, all five bases were identified as P-site interactions on the basis of chemical footprinting and modification-interference experiments (20, 41, 42). C1400 appears to stabilize the wobble base pair by stacking on base 34 of tRNA, an arrangement that was predicted by Ofengand and co-workers nearly 20 years ago, from photochemical cross-linking studies (43).

The minor groove of helix 69 of 23S rRNA, which forms bridge B2a, interacts with the minor groove of the D stem of P-tRNA (Fig. 6E; interaction g), extending into the A site where its conserved loop interacts with almost the same features of the D stem of A-tRNA (Fig. 7D; interaction f), as well as forming the B2a bridge contact with the top of the penultimate stem (Fig. 5D). This complex set of interactions explains chemical footprinting results that showed partial protection of bases in the 1915 loop of helix 69 by the 30S subunit, which became complete upon binding of tRNA (35). At its elbow, a  $\beta$ -hairpin loop of protein L5 (positions 54 to 66) interacts with the T loop of P-tRNA at the minor-groove face of C56 (Fig. 6E; h). The CCA tail of the P-tRNA is positioned to allow the predicted C74-G2252 base pairing with the 23S rRNA P loop (44), observed in the recent high-resolution structure of the archaeal 50S subunit complexed with substrate analogs (3). In addition, the acceptor end is positioned by a backbone-backbone contact between the acceptor stem and the stem of the 23S rRNA P loop (Fig. 6E; i) and interactions between the CCA tail and nucleotides A2602 and U2585, both of which have been implicated in the peptidyl transferase function of the large subunit (35, 45).

Recently, the atomic-resolution structure

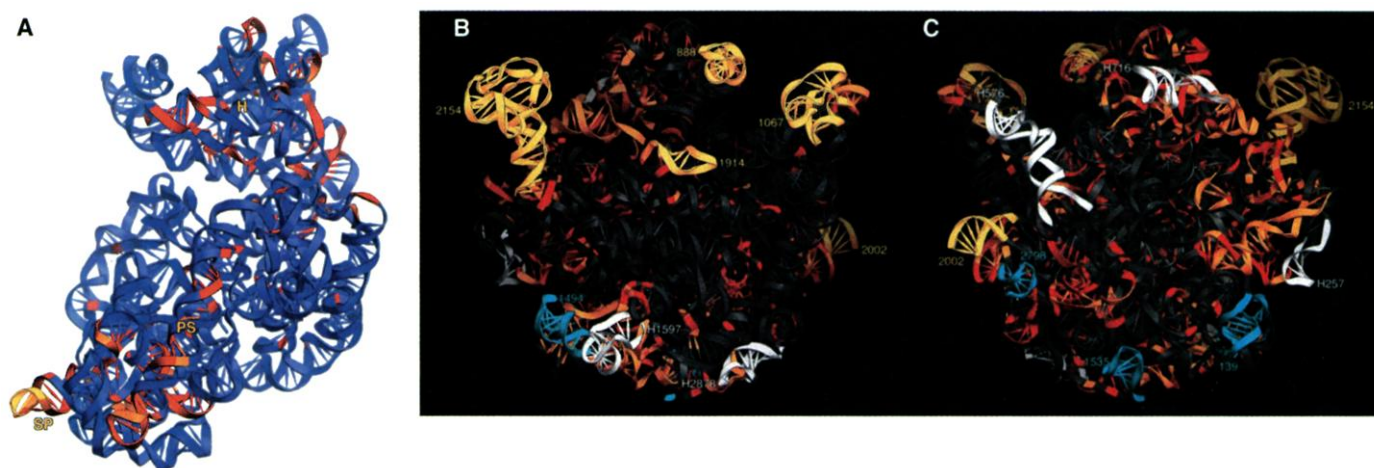


**Fig. 4.** Conformational differences between rRNAs in 70S ribosomes and 30S and 50S subunits. (A) Differences in 16S rRNA from *T. thermophilus* 30S subunits (14) and 70S ribosomes. Differences are colored yellow (>10 Å), orange (5.5 Å to 10 Å), red (3.5 Å to 5.5 Å), and blue (<3.5 Å). H, head; PS, penultimate stem; SP, spur. (B and C) Front and back views of the 23S rRNA, showing differences between the *H. marismortui* 50S subunit (13) and the *T. thermophilus* 70S

ribosome. Yellow, features that were disordered in the *H. marismortui* 50S structure; cyan, features that are specific to the *T. thermophilus* structure; white, features specific to the *H. marismortui* structure. Conformational differences in the remaining regions are colored orange (>5.5 Å) and red (3.5 Å to 5.5 Å). Nucleotide numbers of *Haloarcula*-specific features are preceded by H; the remaining numbers are according to *E. coli* numbering.

of the *Haloarcula* 50S subunit has been solved in complex with the compound CCdAp-Puromycin (3), which is believed to be a transition-state analog of the peptidyl transferase reaction (46). This structure has led to a proposal for a mechanism for catalysis of peptide bond formation by the ribosome (3). At 5.5 Å resolution, most of the conformation of the rRNA backbone in the vicinity of the 3'-CCA end of P-site tRNA shows few discernible differences between the two structures. The few apparent differences are localized to the P loop and around positions 2451, 2506, 2585, and 2602, which may move in a concerted way. In the 70S ribosome complex, the position of the 3'-CCA end of the P-tRNA, relative to nearby features of 23S rRNA, appears to differ from that of the corresponding part of the transition-state analog, possibly because of the absence of an acyl group.

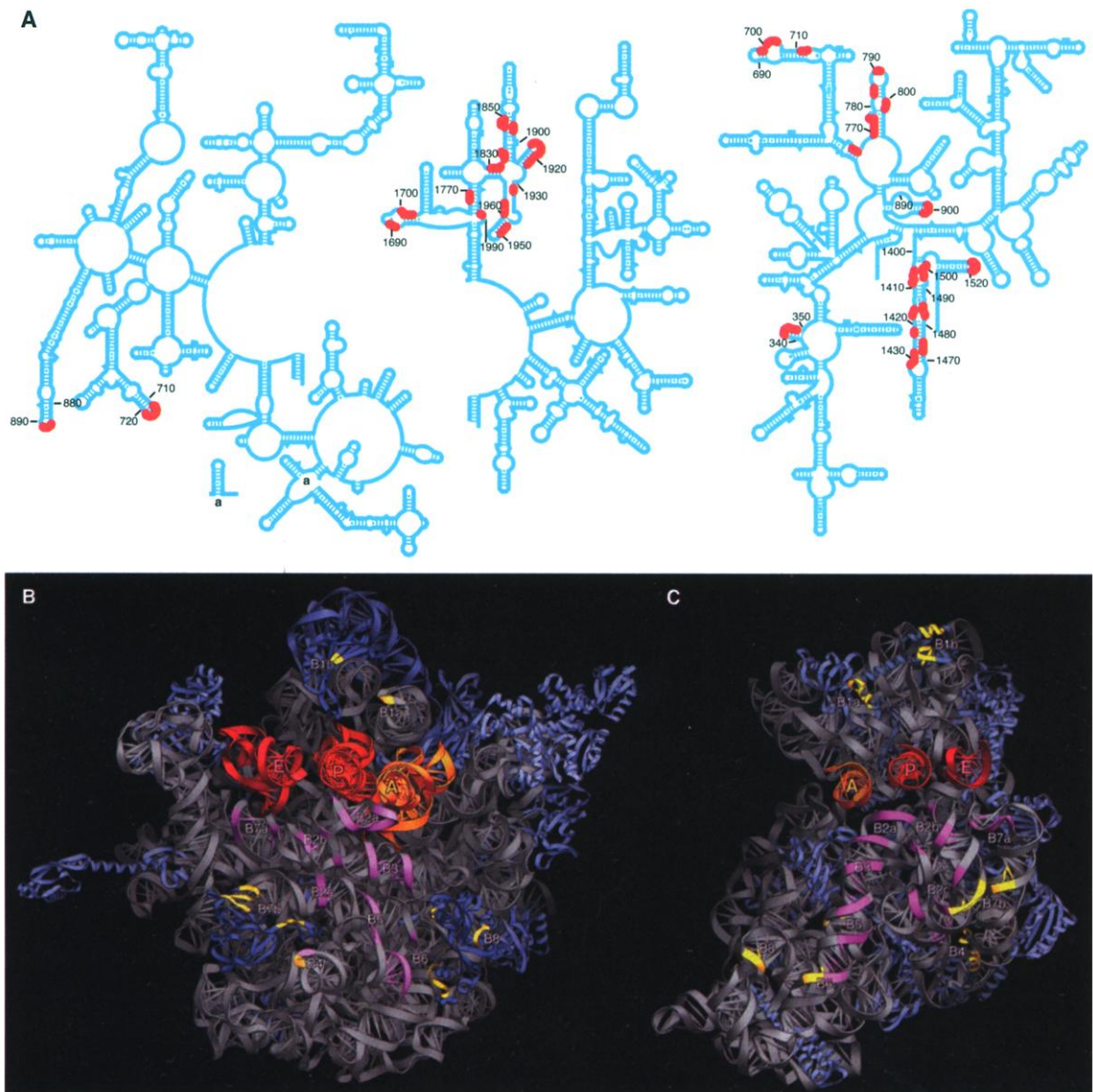
Surrounding the A-tRNA anticodon

loop in the 30S subunit are G530, A1492, and A1493, the three universally conserved bases originally identified as A-site-specific features by chemical footprinting studies (20, 42) and shown to affect A-site binding by mutational and biochemical studies (47, 48). All three bases are positioned close to the site of codon-anticodon interaction in the 30S A site (Fig. 7, A and B; a and d). The tRNA-protected N1 positions of bases A1492 and 1493 point away from the codon-anticodon base pairs and are separated from them by the 16S rRNA backbone, when the 30S subunit A site is vacant (14), consistent with the electron density of the 70S ribosome in the absence of A-tRNA. In the presence of the aminoglycoside antibiotic paromomycin, the conformations of nucleotides 1492 and 1493 have been found to rearrange (16), raising the possibility that they may also rearrange in response to binding tRNA to the 30S A site. In the 7 Å

Fourier difference map of the A-site tRNA bound to the 70S ribosome (Fig. 7C), a patch of negative electron density is seen at the position of bases 1492-1493, providing support for the possibility that they rearrange to interact with the first and second base pairs in the minor groove of the A-site codon-anticodon helix, as suggested by Carter *et al.* (16). The N1 position of G530 is also protected upon A-tRNA binding (20, 42) and mutations of this base confer a dominant lethal phenotype and defective A-tRNA binding (47). G530 is also positioned in the minor groove of the codon-anticodon helix, near the second and third base pairs. The bulged base C1054, mutations in which have been shown to suppress UGA nonsense mutations (49), projects toward the apex of the A-tRNA anticodon loop (Fig. 7B; b).

Lysine 120 of protein S13 and phosphate 955 are both close enough to interact

**Fig. 5. Intersubunit bridges.** (A) Secondary structures of 16S and 23S rRNAs, showing features involved in intersubunit contacts (red). (B and C) Interface views of the 50S and 30S subunits, with the bridges numbered (5, 11). RNA-RNA contacts are shown in magenta; protein-RNA and protein-protein contacts are shown in yellow. The bridge contact B1b with protein L5 is not explicitly modeled, but its approximate position is indicated in the figure. A, P, and E indicate the three tRNAs (23S rRNA) or tRNA anticodon stem loops (16S rRNA). (D to G) Detailed stereo views of the bridge interactions, viewed as in (D) Fig. 1B, (E) Fig. 1C, (F) Fig. 1D, rotated 90° around the horizontal axis, and (G) Fig. 1D.



with the tRNA backbone around position 41 (Fig. 7, A and B; c). The conserved lobe of S12, which bears the universal PNSA sequence around position 50, projects into the space between the 530 loop and the 1492-1493 strand of the decoding site (Fig. 7A; e), completing the floor of the 30S subunit A site. Mutations on the right-hand side of the lobe, facing the top of the penultimate stem at nucleotides 1492 and 1493 and the switch helix (50), at positions 910 to 912, confer restrictive (hyperaccurate) phenotypes [reviewed in (51)]. These mutations could have the effect of widening the space between the 530 loop and 1492-1493 strands, loosening the interactions between the tRNA-mRNA complex and the 30S A site.

The elbow of A-tRNA interacts with bridge B1a (the A-site finger; H38) at its D and T loops (Fig. 7D; g) and with protein

L16 (l). Protein L11 and its associated RNA near position 1067 of 23S rRNA (H43) (52), although not directly interacting with the A-tRNA, are close to its T loop and could contact it transiently with only modest movement of either the tRNA or 23S rRNA. Electron density from protein L16 or an as-yet- unidentified ribosomal protein partially occupies the position of the A-tRNA elbow (Fig. 7E) and so must move upon A-tRNA binding, possibly as part of the "accommodation" step (53). Helix 89 of 23S rRNA runs nearly parallel to the acceptor arm of the A-tRNA, making a minor-groove interaction (h) with the T stem at the top, and contacting the backbone of the CCA tail that lies across the major groove of its noncanonical helical extension (j) at the bottom. The CCA tail is also positioned by contact with the conserved 1942 loop, which tucks into the

major groove at the end of the acceptor stem (i), and by the previously predicted base pair between C75 and G2553 of 23S rRNA (54), observed in the 50S crystal structure (3).

The E-tRNA anticodon stem loop is wedged between the head and platform of the 30S subunit, where it is surrounded by a dense system of molecular interactions (Fig. 8A). Helices 28 and 29 of 16S rRNA as well its 690 and 790 loops contribute RNA contacts a to e (Fig. 7E). The COOH-terminal  $\alpha$ -helix of protein S7 packs against the backbone of the anticodon stem, whereas the S7  $\beta$ -hairpin is positioned at the Watson-Crick face of the E-tRNA anticodon (f). Although normal codon-anticodon interaction is absent, there may be contact between the second base of the noncognate E-tRNA anticodon and the mRNA.

Protein L1 and its binding region (H76-77) on 23S rRNA interact with the elbow of E-tRNA (contacts g to i). The E-tRNA-protected bases G2112 and G2116 may stack on the tertiary G19-C56 base pair at the top of the tRNA elbow. The acceptor stem makes a minor-groove interaction with helix 68 of 23S rRNA, which includes the backbone contacts with ribose 71 that have been shown by Joseph and co-workers to be essential for EF-G-dependent translocation (55). In addition, the conserved A1853 may make an A-minor interaction with the 2-71 base pair. The CCA tail is buried in a deep pocket of the 50S subunit that is separate from the peptidyl transferase cleft, making contacts with helices 11, 74, and 75 of 23S rRNA and protein L33 and the E-tRNA-protected C2394 (35). The blockage of the exit path for the E-tRNA by protein S7 and by L1 and its rRNA binding site requires that one or both of these structures move to allow release of the deacylated tRNA. Rotation of the head of the 30S subunit (see below) and the observed mobility of the L1 region of yeast 80S ribosomes (56) support both possibilities.

**Implications for the mechanism of translation.** The structure of a complete ribosome provides the basis for understanding the mechanism of protein synthesis at the molecular level. The dynamic nature of this process implies that the ribosome contains moving parts that enable its function (57). The translocation step of protein synthesis inescapably requires movements of 20 Å or more by the tRNAs, as they move from the A to P to E sites. It seems unlikely that such movements would not be matched by corresponding structural rearrangements of the ribosome (58). The hybrid states model, in which the tRNAs move independently with respect to the 30S and 50S

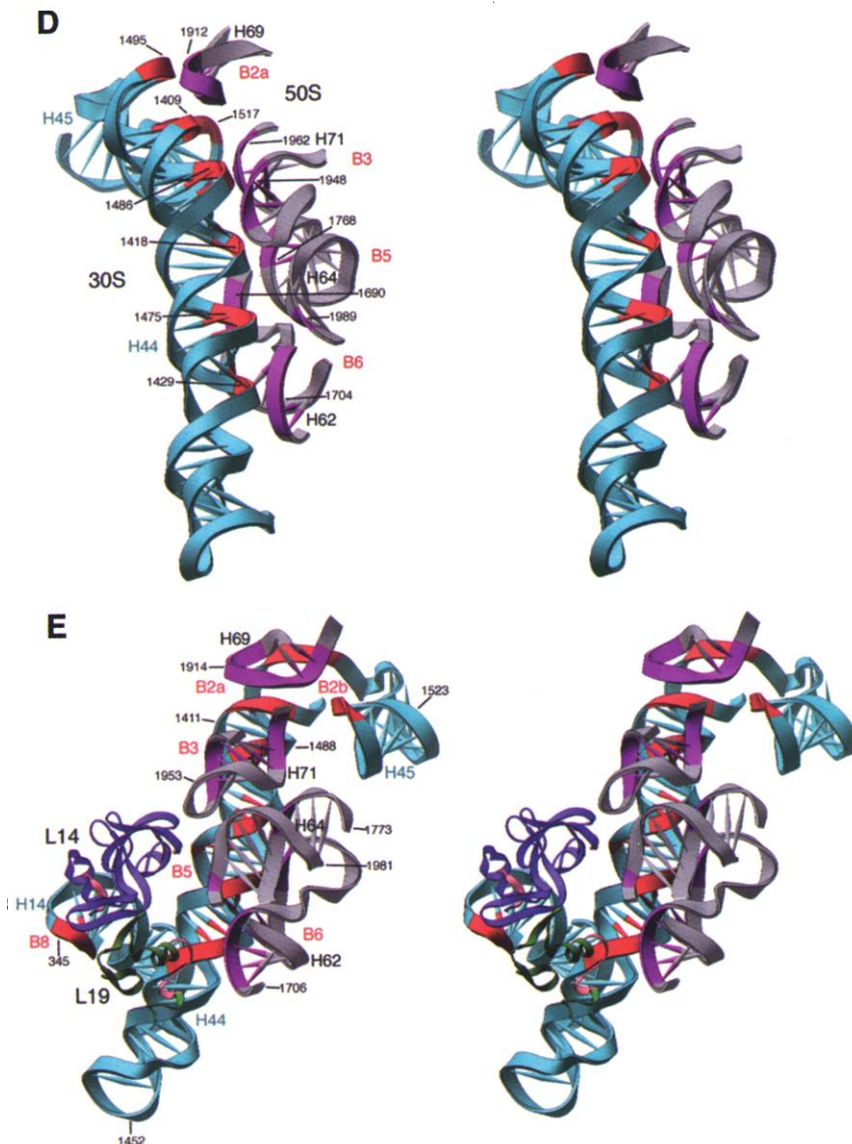


Fig. 5. (continued).

subunits in two separate steps, carries the implication that the mechanism of translocation may involve relative movement of the 30S and 50S subunits or of particular structural domains or substructures of the two subunits (37). Thus far, most of the evidence for movement has pointed mainly to the 30S subunit. Neutron scattering experiments, in which changes in the radius of gyration of the ribosome were observed between the pre- and posttranslocation states, suggested movement of the head of the small subunit (26). Cryo-EM comparison of ribosomes bearing mutations in the “switch helix” (helix 27) of 16S rRNA indicates conformational differences in the head, shoulder, platform, and penultimate stem of the 30S subunit between the ram and restrictive forms (59). Comparison of the conformation of 16S rRNA in the 70S ribosome with that of the separate 30S subunit (Fig. 3, A and B) again shows differences that suggest mobility of the head, platform, and penultimate stem regions of the small subunit. Recent cryo-EM studies (60, 28) indicate rotation of the entire 30S subunit by about 6° upon binding of EF-G-GTP.

The hybrid states implication that tRNA translocation may involve relative movement at the subunit interface was reinforced by the observation that many of the nucleotides implicated in tRNA-ribosome interactions by biochemical and genetic experiments are adjacent to nucleotides involved in subunit association (17, 18). The crystal structure provides direct evidence for close proximity of the tRNA binding sites to interface contacts and even shows that some of the bridges interact directly with the tRNAs. Moreover, there is evidence that some of these tRNA-bridge interactions are dynamic. Among the structural elements that are disordered in the 50S subunit structure are the bridges B1a, B1b, and B2a. The disorder is informative in that it identifies specific molecular features of the ribosome that are capable of independent motion, at least under conditions prevailing in the crystal, and so are candidates for participation in ribosomal dynamics. B1a and B1b connect the central protuberance of the 50S subunit to the head of the 30S subunit (Figs. 2E and 5, B and C; Table 2), an independent structural domain that has repeatedly been implicated in ribosomal dynamics, as discussed above. Bridges B1a and B1b contact the conserved elbow regions of the A- and P-tRNAs, respectively, which undergo the largest movement (~40 to 50 Å) during translocation. Helix 38 of 23S rRNA, around its conserved internal loop at positions 882/898, interacts with the D and T loops of A-tRNA, and protein L5 interacts with the T loop of P-tRNA through the conserved β-hairpin centered on residue 80. B1a

and B1b are also the bridges most strongly affected by the EF-G-dependent intersubunit rotation observed in the above-mentioned cryo-EM studies (28). Near their junctions with the body of the 50S subunit, these two bridges are straddled by 5S rRNA, which might in some way help to coordinate their movement.

The most intriguing of the flexible bridge elements is the centrally located B2a, formed by interaction of the universally conserved 1915 loop of helix 69 of 23S rRNA with the top of the penultimate stem (helix 44) of 16S rRNA at the base of the decoding site, where codon-anticodon interactions take place. The helix 69 stem loop also contacts the A- and P-tRNAs, its loop interacting simultaneously with the penultimate stem of 16S rRNA and with the minor groove of the D stem of A-tRNA, whereas the minor groove of its stem contacts the minor-groove surface of the D stem of the adjacent P-tRNA. The disorder of helix 69 in the 50S subunit structure can be explained by the absence of any direct stacking or other packing interactions with the 50S subunit and its connection to the rest of 23S rRNA by only a single-stranded loop, to the conserved lateral arm of domain IV of 23S rRNA (which, in turn, embodies bridges B2b, B3, and B7a; Fig. 5C). Continuous coaxial stacking of the

lateral arm includes a noncanonical helix that occupies nearly a whole helical turn in the highly conserved region separating the Watson-Crick helices 68 and 71 (bridges B2b and B3) just below and directly parallel to helix 69. In this crucial central region of the interface, it is not difficult to see how the movement of tRNA could be coupled to perturbation of the interface contacts at bridges B2a, B2b, and B3 and potentially to conformational rearrangement of the noncanonical helical segment of the lateral arm. In the posttranslocation state, directed hydroxyl radical probing (58) and cryo-EM studies (61) placed helix 69 in proximity to the tip of the functionally dynamic domain IV of elongation factor EF-G, which is believed to mimic tRNA (62) and has been implicated in the mechanism of EF-G-catalyzed tRNA movement (61).

Interaction of the 1915 loop of helix 69 with the minor groove of the D stem of A-site tRNA suggests a possible explanation for the mechanism of action of the Hirsh suppressor (63), one of the more puzzling tRNA nonsense-suppressor mutations, consisting of an A to G mutation at position 24 in the D stem of tryptophan tRNA. A24 is base paired to U11, which is nearly always a pyrimidine, whose O2 position projects into the minor groove of the D stem, where it is within contact range of

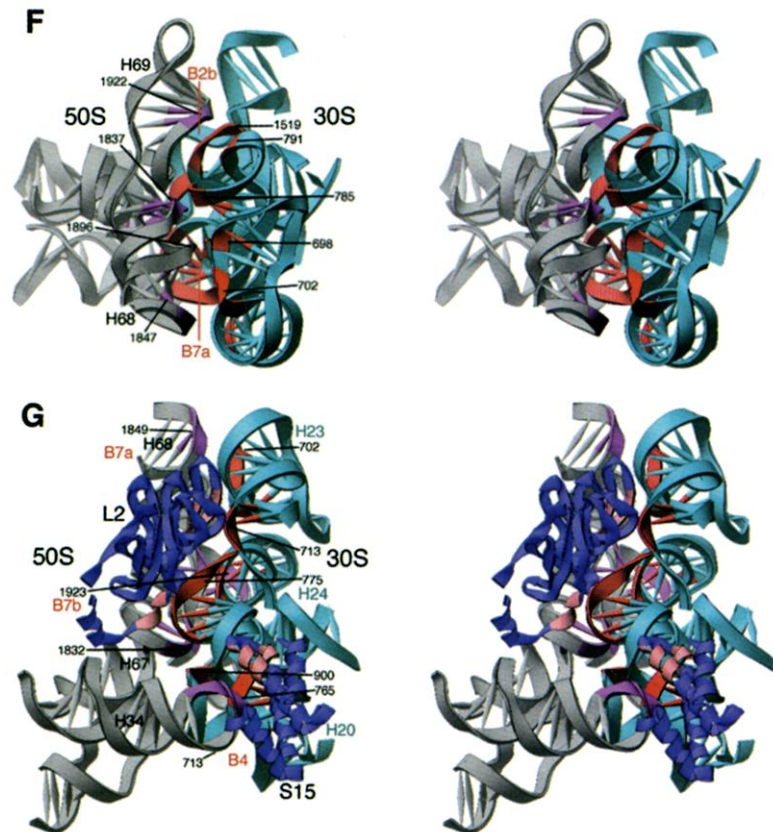


Fig. 5 (continued).

the 1915 loop. Creation of a G24-U11 wobble pair could thus hinder the accessibility of the pyrimidine O2 from the minor-groove side. Dahlberg and co-workers have discovered that mutation of the nearby

C1914 to U confers a nonsense-suppressor phenotype (64). Thus, this unanticipated bridge B2a-tRNA interaction may play an important role in translational fidelity.

The other bridges implicated in ribo-

somal function involve the penultimate stem (helix 44), switch helix (helix 27), and the platform (helices 23 and 24) of 16S rRNA. These three features contain five of the six class III sites, whose interesting

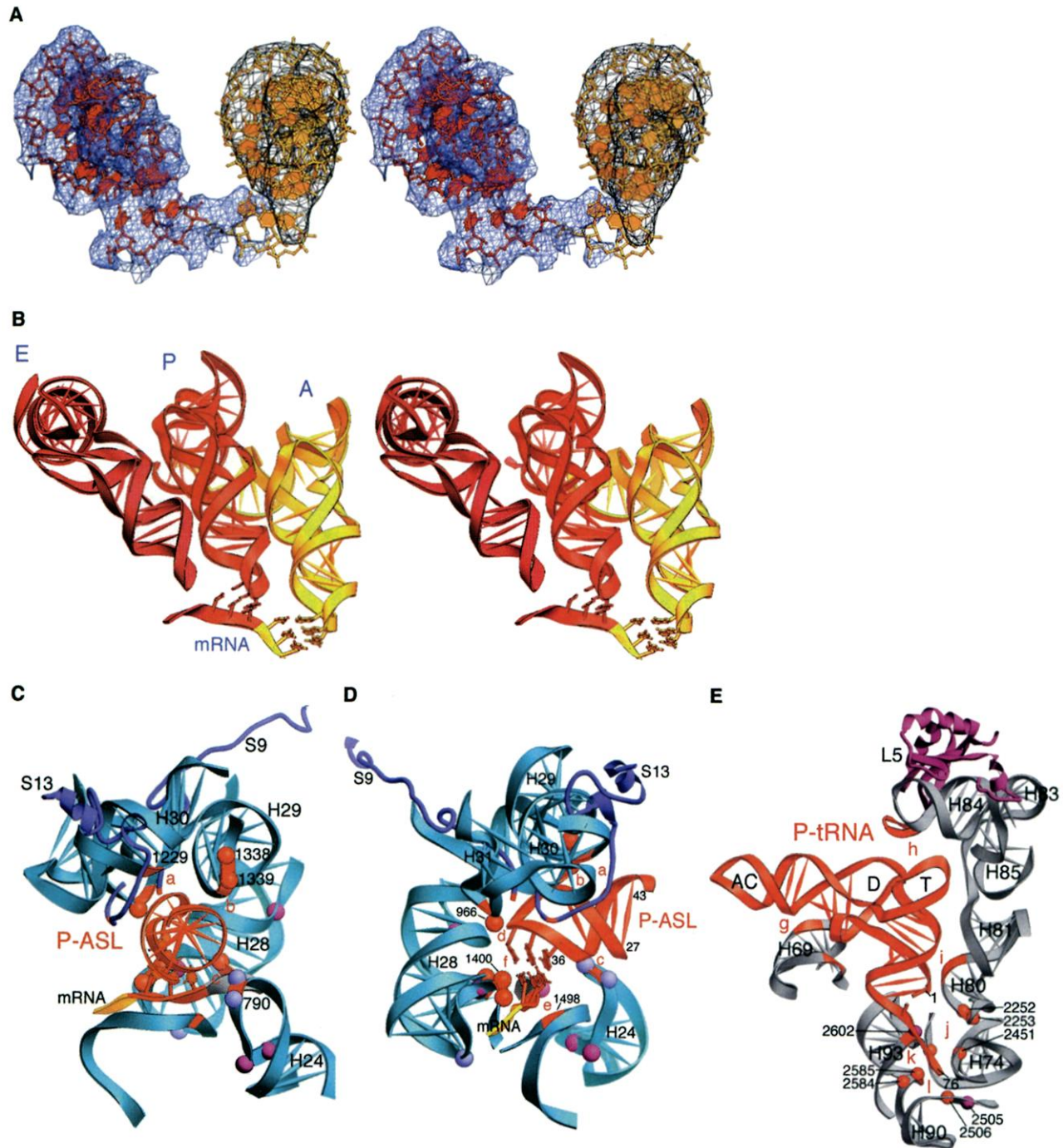


**Fig. 6.** tRNA-ribosome interactions. In all panels, 16S rRNA is shown in cyan, 23S rRNA in gray, and ribosomal proteins in blue and magenta. Parts of the ribosome that contact the tRNAs are colored gold (A-tRNA contacts), orange (P-tRNA contacts), or red (E-tRNA contacts). rRNA helices are numbered as in Fig. 3, A and B. Bases in rRNA that are protected from chemical probes by tRNA binding (20, 35, 42) are indicated by spheres. Bases that are protected by direct interaction are colored the same as the contacts; bases that are protected as a result of conformational changes are shown in magenta or, in the case of class III sites (65), gray-blue. The different specific ribosome contacts discussed

in the text and listed in Table 3 are indicated by lowercase letters. (A) Stereo electron density maps of the P-tRNA (left; 5.5 Å) and A-tRNA (right; 7 Å) complexed with their respective mRNA codons in the 70S ribosome. (B) Stereo diagram of the relative orientations of the A-, P-, and E-tRNAs (gold, orange, and red, respectively) and mRNA, showing codon-anticodon interactions and the kink between the A and P codons. (C and D) Two views of the P-tRNA anticodon stem-loop bound to its codon in the 30S subunit P site. (E) Interactions between the D stem, elbow, and acceptor arm of P-tRNA with the 50S subunit.



RESEARCH ARTICLES

behavior was identified in earlier chemical probing experiments (65). These bases are all protected independently by tRNA, 50S

subunits, or certain antibiotics. The observation that all three kinds of ligand were independently able to protect these bases

led to the conclusion that their protection must be caused by ligand-induced conformational changes rather than direct contact between the bases and ligands. Indeed, the structural results show that none of these bases make direct contact with the 50S subunit, tRNA, or antibiotics (16, 66). Three class III sites (A909, A1413, and G1487) are found at the contact surface between the internal loop of the switch helix with the minor groove of the penultimate stem, where A909 makes an A-minor interaction with the noncanonical A1413-G1487 base pair (14). The reactivities of the N1 positions of all three purine bases in vacant 30S subunits indicates that interaction with tRNA, 50S subunits, or streptomycin or the neomycin-related antibiotics induces formation of this interhelical base-triple interaction. Protection by subunit association can be explained by the bridge interactions B2a and B3, which directly flank the 1413-1487 pair, and B2c, which involves the 900 loop of the switch helix. Protection by tRNA and antibiotics is consistent with binding of the A- and P-tRNAs and drugs to the decoding site at the top of the penultimate stem. The two class III bases in the 790 loop are protected by their interactions with the 16S rRNA backbone in the decoding site at positions 1497-1498, next to the P-site codon-anticodon interaction. This interaction appears to be stabilized upon subunit association by contact of helix 24 of 16S rRNA with the 50S subunit in the adjacent bridge B2b and as a result of tRNA binding by backbone-backbone interactions between positions 790-791 and nucleotides 38-39 in the P-tRNA anticodon stem-loop. The sixth class III base is A1394, in the neck of the subunit (helix 28), in which a hydrogen bond is formed between the N1 position of A1394 and the 2'-hydroxyl of the decoding site nucleotide A1500 (14). The global result of the class III conformational changes appears to be an overall tightening of the base of the decoding site, in the channel where the mRNA is bound and where the A- and P-site codon-anticodon interactions take place, which could help to explain the miscoding effects of streptomycin and the aminoglycoside antibiotics.

Intramolecular movement in 16S rRNA, embodied in the class III conformational changes, can be linked to at least one mobile element of 23S rRNA, the conserved 1915 stem loop (helix 69), and the potentially mobile noncanonical helix in the middle of the lateral arm of domain IV, which is flanked by bridges B2a, B2b, B2c, and B3. As just discussed, all four of these bridges are implicated in 50S-induced conformational changes in 16S rRNA that are manifested by the class III protections. It would not be surprising to find

**Table 3.** tRNA-ribosome contacts. AC, anticodon; acc., acceptor; D loop, D stem, the dihydrouracil loop and stem of tRNA; T loop, T stem, the thymidine-containing loop and stem of tRNA. RNA contacts are indicated as follows: bk, backbone; bs, base; bp, base pair. Where results are inconclusive, the designation is omitted. tRNA positions are numbered according to yeast tRNA<sup>Phe</sup>; rRNA positions are numbered according to *E. coli*.

	Interaction	tRNA positions	Ribosome positions
<b>P site</b>			
a	AC stem-16S (H30)	28-30 bk	16S (1229)bk
	AC stem-513	36 bk	S13 (116-120)
b	AC stem-16S (L29-42)	40 bk	16S (1339) bk
		40 bs	16S (1339) bs
		41 bs	16S (1338) bs
c	AC loop-16S (790 loop)	38 bk	16S (790) bk
d	AC loop-16S (965 loop)	34 bk	16S (m <sup>2</sup> C966) bs
	AC loop-S9	35 bk	S9 (R128)
e	P codon-16S (decoding site)	*P codon 1 bk	16S (926)bs
			16S (1498) bk
f	AC loop-16S (decoding site)	34 bs	16S (1400) bs
g	D stem-23S (H69)	12, 13 bk	23S (1908-1909) bk
		25, 26 bk	23S (1922-1923) bk
h	T loop-L5	56-7	L5 (55-66)
i	acc. stem-23S (P stem/H80)	3 bk	23S (2255-2256) bk
j	acc. tail-23S (P loop)	74 bs	23S (2252) bs
k	acc. tail-23S (H93)	75	23S (2602)
l	acc. tail-23S (L90-93)	76	23S (2585)
<b>A site</b>			
a	Codon-anticodon helix-16S (530 loop)	34-35 bs	16S (530) bs
		36 bk	16S (530) bk
b	AC-16S (H34)	34 bk	16S (1054) bs
c	AC stem-16S (965 loop)	40 bk	16S (955) bk
	AC stem-513	40-41 bk	S13 (120-122)
d	AC loop-16S (decoding site)	38 bk	16S (1493) bk
	A codon-16S (dec. site)	*A codon 1 bk	16S (1493) bk
e	A codon-S12	*A codon 2, 3 bk	S12 (46-48)
f	D stem-23S (H69)	11, 12	23S (1914-1915)
	D stem junction-23S (H69)	25, 26	23S (1913-1914)
g	D loop-23S (A-site finger/H38)	D17 bs	23S (881-882) bk
		G 19 bs	23S (882-883) bk
	T loop-23S (A site finger/H38)	56 bk	23S (898-899) bk
h	T stem-23S(H89)	50-53 bk	23S (2470-2472) bk
		64-65 bk	23S (2482-2484) bk
		72-73	23S (1942-1943)
i	acc. stem-23S (H71)	74-76 bk	23S (2452, 2494) bk
j	acc. tail-23S (H89)	75 bs	23S (2553) bs
k	acc. tail-23S (A loop)	55,62	L16 (27, 30)
l	T stem-loop-L16		
<b>E site</b>			
a	AC loop-16S (H29)	35, 36 bk	16S (1339, 1340) bk
	AC stem-16S (L29-42)	30 bk	bk
b	AC loop-16S (H28)	34 bk	16S (1382) bk
c	AC loop-16S (L28-29)	33 bk	16S (937) bk
d	AC loop-16S (790 loop)	37-38 bk	16S (788-789) bk
e	AC loop-16S (690 loop)	37 bs	16S (693) bs
		38-39 bk	16S (694-695) bk
f	AC loop-S7	37	S7 (β-hairpin)
		42	S7 (α-helix 6)
g	D loop-23S (L76-77)	19	23S (2112-2113)
h	T loop-23S (L76-77)	56	23S (2116-2117)
	T loop-L1	56-57	L1 (124-128)
i	T stem-L1	G53-C61 bp	L1 (52-54)
	T loop-L1	55 bk	L1 (165-169)
j	acc. Stem-23S (H68)	2-71 bp	23S (1852-1853) bs
		71 bk	23S (1892) bk
		3-5 bk	23S (1850-1853) bk
k	acc. Tail-23S (H75)	73 bk	23S (2235) bk
l	acc. Tail-23S (H74)	76 bk	23S (2433-2434)
m	acc. Tail-23S (H11)	76 bs	23S (199) bs
n	acc. Tail-L33	73-74	L33

\*Interaction with mRNA backbone.

that these same conformational changes, which are also induced in 16S rRNA by tRNA and mRNA interactions in the decoding site of the 30S subunit, could reciprocally affect the conformation of this interface region of 23S rRNA, through the same set of bridge interactions. This could have interesting implications for the mechanism of translation, because the lateral arm of domain IV packs directly against the 2600 stem loop (helix 93) and the A loop (helix 92) of 23S rRNA, both of which are directly involved in interactions in the peptidyl transferase center (3, 35, 54, 67). Furthermore, the 2563-2564 loop at the base of helix 92 interacts directly with the base of helix 95, the sarcin-ricin loop, which is directly implicated in the activities of elongation factors EF-Tu and EF-G. Finally, the far left-hand end of the lateral arm of domain IV, near bridge B7a, makes interactions with the acceptor end of the E-tRNA that have been shown to be crucial for EF-G-dependent translocation (55). Knowledge of the structure of the complete ribosome complexed with mRNA and tRNA now provides the possibility to test these and other specific molecular models for the mechanism of translation.

## References and Notes

- H. F. Noller, V. Hoffarth, L. Zimniak, *Science* **256**, 1416 (1992).
- R. Green, H. F. Noller, *Annu. Rev. Biochem.* **66**, 679 (1997).
- P. Nissen, J. Hansen, N. Ban, P. B. Moore, T. A. Steitz, *Science* **289**, 920 (2000).
- A. T. Matheson, P. P. Dennis, J. E. Davies, W. E. Hill, *Biochem. Cell Biol.* **73** (1995); R. A. Garrett et al., Eds., *The Ribosome* (American Society for Microbiology, Washington, DC, 2000); W. E. Hill et al., Eds., *The Ribosome: Structure, Function and Evolution* (American Society for Microbiology, Washington, DC, 1990).
- J. Frank et al., *Biochem. Cell Biol.* **73**, 757 (1995).
- M. Stöffler-Meilecke, G. Stöffler, in *The Ribosome: Structure, Function and Evolution*, W. E. Hill et al., Eds. (American Society for Microbiology, Washington, DC, 1990), pp. 123-133; M. O. Oakes, A. Scheinman, T. Atha, G. Shankweiler, J. A. Lake, in *The Ribosome: Structure, Function, and Evolution*, W. E. Hill et al., Eds. (American Society for Microbiology, Washington, DC, 1990), pp. 180-193.
- R. K. Agrawal et al., *Science* **271**, 1000 (1996); H. Stark et al., *Cell* **88**, 19 (1997); H. Stark et al., *Nature* **389**, 403 (1997); R. Matadeen et al., *Structure Fold Design* **7**, 1575 (1999).
- I. S. Gabashvili et al., *Cell* **100**, 537 (2000).
- M. M. Yusupov, M. B. Garber, V. D. Vasiliev, A. S. Spirin, *Biochimie* **73**, 887 (1991); K. von Bohlen et al., *J. Mol. Biol.* **222**, 11 (1991); S. Trakhanov et al., *J. Mol. Biol.* **209**, 327 (1989); I. Makowski et al., *J. Mol. Biol.* **193**, 819 (1987).
- N. Ban et al., *Cell* **93**, 1105 (1998); A. Tocilj et al., *Proc. Natl. Acad. Sci. U.S.A.* **96**, 14252 (1999).
- J. H. Cate, M. M. Yusupov, G. Z. Yusupova, T. N. Earnest, H. F. Noller, *Science* **285**, 2095 (1999).
- W. M. Clemons et al., *Nature* **400**, 833 (1999).
- N. Ban, P. Nissen, J. Hansen, P. B. Moore, T. A. Steitz, *Science* **289**, 905 (2000).
- B. T. Wimberly et al., *Nature* **407**, 327 (2000).
- F. Schluenzen et al., *Cell* **102**, 615 (2000).
- A. P. Carter et al., *Nature* **407**, 340 (2000).
- C. Merryman, D. Moazed, G. Daubresse, H. F. Noller, *J. Mol. Biol.* **285**, 107 (1999).
- C. Merryman, D. Moazed, J. McWhirter, H. F. Noller, *J. Mol. Biol.* **285**, 97 (1999).
- P. Mitchell, M. Osswald, R. Brimacombe, *Biochemistry* **31**, 3004 (1992).
- D. Moazed, H. F. Noller, *Cell* **47**, 985 (1986).
- A. Malhotra et al., *J. Mol. Biol.* **280**, 103 (1998).
- A. T. Brünger et al., *Acta Crystallogr. D Biol. Crystallogr.* **54**, 905 (1998).
- After fitting the backbone of 16S rRNA in our electron density map, high-resolution structures of 30S subunits appeared (14, 15). Our original model differed from the structure of Wimberly et al. (14) by 5.7 Å rmsd and by 7.0 Å from the structure of Schluenzen et al. (15). After correction of errors in register, our structure was within 2.7 Å and 5.2 Å rmsd, respectively, of the same two structures. Availability of the *Haloarcula* 50S subunit structure (13) facilitated fitting the 50S subunit portion of our electron density in regions that are conserved between the bacterial and archaeal structures; initial rigid-body docking of large fragments of the archaeal structure was followed by detailed fitting of smaller fragments and individual phosphates to our map. Small subunit proteins were docked initially as rigid bodies with the coordinates for the individual proteins from the *T. thermophilus* 30S subunit structure (14). Structures for most of the *T. thermophilus* large subunit proteins are not known; therefore, the structures of proteins from the most closely related organisms were modeled, after deleting any extra residues. Details of the fitting of the ribosomal proteins will be presented elsewhere.
- C. R. Woese et al., *Nucleic Acids Res.* **8**, 2275 (1980); R. R. Gutell, *Nucleic Acids Res.* **22**, 3502 (1994).
- See [www.rna.icmb.utexas.edu/](http://www.rna.icmb.utexas.edu/)
- I. Serdyuk et al., *Biochimie* **74**, 299 (1992).
- M. Mougél et al., *J. Mol. Biol.* **198**, 91 (1987).
- J. Frank, R. K. Agrawal, *Nature* **406**, 318 (2000).
- H. F. Noller et al., *Nucleic Acids Res.* **9**, 6167 (1981); R. R. Gutell, M. W. Gray, M. N. Schnare, *Nucleic Acids Res.* **21**, 3055 (1993).
- Differences between the positions of phosphorus atoms were calculated after carrying out least-squares superimpositions of the respective 16S (14) and 23S rRNAs (13) as follows. First, a distance matrix was calculated independently for each RNA coordinate set. Then a set of the 214 atoms whose intramolecular distance values varied the least between the two comparison molecules was used to superimpose the entire molecules by a least-squares fit, with the program MIDAS [T. E. Ferrin, C. C. Huang, L. E. Jarvis, R. Langridge, *J. Mol. Graphics* **6**, 13 (1988)].
- W. Herr, N. M. Chapman, H. F. Noller, *J. Mol. Biol.* **130**, 433 (1979).
- G. M. Culver, J. H. Cate, G. Z. Yusupova, M. M. Yusupov, H. F. Noller, *Science* **285**, 2133 (1999).
- P. Nissen, J. A. Ippolito, N. Ban, P. B. Moore, T. A. Steitz, *Proc. Natl. Acad. Sci. U.S.A.* 10 April 2001 (eprint ahead of print).
- B. S. Cooperman, T. Wooten, D. P. Romero, R. R. Traut, *Biochem. Cell Biol.* **73**, 1087 (1995); M. Uhlein, W. Weglohner, H. Urlaub, B. Wittmann-Liebold, *Biochem. J.* **331**, 423 (1998).
- T. Döring, P. Mitchell, M. Osswald, D. Bockkariov, R. Brimacombe, *EMBO J.* **13**, 2677 (1994); S. Joseph, H. F. Noller, *EMBO J.* **15**, 910 (1996); S. Joseph, B. Weiser, H. F. Noller, *Science* **278**, 1093 (1997).
- D. Moazed, H. F. Noller, *Cell* **57**, 585 (1989).
- L. Jovine, S. Djordjevic, D. Rhodes, *J. Mol. Biol.* **301**, 401 (2000).
- D. Moazed, H. F. Noller, *Nature* **342**, 142 (1989).
- At the present resolution, actual atomic interactions are not resolved. However, known RNA stereochemistry, combined with the docked high-resolution structures, strongly constrains, for example, whether interactions with RNA involve the sugar-phosphate backbone or the bases and in some cases allows us to predict which chemical groups are most likely to be involved.
- W. Schnitzer, U. von Ahnsen, *Proc. Natl. Acad. Sci. U.S.A.* **94**, 12823 (1997).
- H. F. Noller, J. B. Chaires, *Proc. Natl. Acad. Sci. U.S.A.* **69**, 3113 (1972).
- U. von Ahnsen, H. F. Noller, *Science* **267**, 234 (1995).
- D. Moazed, H. F. Noller, *J. Mol. Biol.* **211**, 135 (1990).
- J. Ofengand, J. Ciesiolka, R. Denman, K. Nurse, in *Structure, Function, and Genetics of Ribosomes*, B. Hardisty, G. Kramer, Eds. (Springer-Verlag, New York, 1986), pp. 473-494.
- R. R. Samaha, R. Green, H. F. Noller, *Nature* **377**, 309 (1995).
- A. Barta, G. Steiner, J. Brosius, H. F. Noller, E. Kuechler, *Proc. Natl. Acad. Sci. U.S.A.* **81**, 3607 (1984).
- M. Welch, J. Chastang, M. Yarus, *Biochemistry* **34**, 385 (1995).
- T. Powers, H. F. Noller, *Proc. Natl. Acad. Sci. U.S.A.* **87**, 1042 (1990).
- S. Yoshizawa, D. Fourmy, J. D. Puglisi, *Science* **285**, 1722 (1999).
- E. J. Murgola, K. A. Hijazi, H. U. Goring, A. E. Dahlberg, *Proc. Natl. Acad. Sci. U.S.A.* **85**, 4162 (1988).
- J. S. Lodmell, A. E. Dahlberg, *Science* **277**, 1262 (1997).
- C. G. Kurland et al., in *The Ribosome: Structure, Function, and Evolution*, W. E. Hill et al., Eds. (American Society for Microbiology, Washington, DC, 1990), pp. 513-526.
- G. L. Conn, D. E. Draper, E. E. Lattman, A. G. Gittis, *Science* **284**, 1171 (1999); B. T. Wimberly, R. Guymon, J. P. McCutcheon, S. W. White, V. Ramakrishnan, *Cell* **97**, 491 (1999).
- T. Pape, W. Wintermeyer, M. Rodnina, *EMBO J.* **18**, 3800 (1999).
- D. F. Kim, R. Green, *Mol. Cell* **4**, 859 (1999).
- J. S. Feinberg, S. Joseph, personal communication.
- M. G. Gomez-Lorenzo et al., *EMBO J.* **19**, 2710 (2000).
- A. S. Spirin, *Cold Spring Harbor Symp. Quant. Biol.* **34**, 197 (1969).
- K. Wilson, H. F. Noller, *Cell* **92**, 337 (1998).
- I. S. Gabashvili et al., *EMBO J.* **18**, 6501 (1999).
- R. K. Agrawal, A. B. Heagle, P. Penczek, R. A. Grassucci, J. Frank, *Nature Struct. Biol.* **6**, 643 (1999).
- R. K. Agrawal et al., *J. Cell Biol.* **150**, 447 (2000).
- P. Nissen et al., *Science* **270**, 1464 (1995).
- D. Hirsh, *J. Mol. Biol.* **58**, 439 (1971).
- M. O'Connor, A. E. Dahlberg, *J. Mol. Biol.* **254**, 838 (1995).
- D. Moazed, H. F. Noller, *Nature* **327**, 389 (1987).
- D. Fourmy, M. I. Recht, S. C. Blanchard, J. D. Puglisi, *Science* **274**, 1367 (1996).
- D. Moazed, H. F. Noller, *Proc. Natl. Acad. Sci. U.S.A.* **88**, 3725 (1991); R. Green, C. Switzer, H. F. Noller, *Science* **280**, 286 (1998).
- B. Weiser, H. F. Noller, unpublished data.
- J. Brosius, T. J. Dull, H. F. Noller, *Proc. Natl. Acad. Sci. U.S.A.* **77**, 201 (1980).
- Z. Otwinowski, in *Data Collection and Processing*, L. Sawyer, N. Isaacs, D. Bailey, Eds. (SERC Daresbury Laboratory, Warrington, UK, 1993), pp. 52-62.
- M. Carson, *Methods Enzymol.* **277B**, 493 (1997).
- T. A. Jones, J. Y. Zou, S. W. Cowan, M. Kjeldgaard, *Acta Crystallogr. A* **47**, 110 (1991).
- We thank L. Lancaster for fitting all of the small subunit ribosomal proteins, A. Szöke, H. Szöke, S. Ray, B. Scott, J. Murray, and C. Wilson for stimulating discussions; R. Gutell and F. Michel for generously providing unpublished sequence analysis results and alignments and for discussions; G. McDermott, K. Henderson, J. Nix, and L.-W. Hung for advice and help with data collection; S. Joseph for communicating unpublished results; and B. Weiser for generating secondary structure figures. Three-dimensional model renderings were generated with RIBBONS (71), the electron density maps with RIBBONS and with O (72), and secondary structure diagrams with XRNA (68). This work was supported by grants from the NIH and the Agouron Institute (to H.F.N.), from the W. M. Keck Foundation (to the Center for Molecular Biology of RNA), and from the Whitehead Institute for Biomedical Research and from the Searle Scholars Program (J.H.D.C.). The Macromolecular Crystallography Facility at the Advanced Light Source, Lawrence Berkeley National Laboratory is supported by the Department of Energy and by grants from the NIH and the Agouron Institute (T.N.E.). Coordinates for the molecular structures have been deposited with the RCSB (PDB accession number 1G1X and 1G1Y).

21 February 2001; accepted 20 March 2001  
 Published online 29 March 2001;  
 10.1126/science.1060089  
 Include this information when citing this paper.